Available online at www.sciencedirect.com
ScienceDirect
International Journal of Thermal Sciences 48 (2009) 860–870
International Journal of Thermal Sciences
www.elsevier.com/locate/ijts

Numerical study of mixed convection on jet impingement cooling in a horizontal porous layer under local thermal non-equilibrium conditions

Kok-Cheong Wong *, Nawaf H. Saeid

School of Mechanical Engineering, University of Nottingham Malaysia campus, Jalan Broga, 43500 Semenyih, Selangor Darul Ehsan, Malaysia

Received 29 February 2008; received in revised form 9 June 2008; accepted 9 June 2008

Available online 7 July 2008

Abstract

The present study numerically investigates the mixed convection arises from jet impingement cooling of an isothermal heated surface immersed in a confined porous channel under local thermal non-equilibrium conditions. The heat transfer characteristics are investigated with a parametric study over wide ranges of governing parameters: the Rayleigh number ($10 \leqslant Ra \leqslant 200$), Péclet number ($1 \leqslant Pe \leqslant 10^4$), Darcy number ($10^{-6} \leqslant Da \leqslant 10^{-3}$), porosity ($0.75 \leqslant \varphi \leqslant 0.99$), heat transfer coefficient between solid and fluid ($1 \leqslant H \leqslant 10^3$), and porosity scaled thermal conductivity ratio ($0.001 \leqslant K_r \leqslant 5$). The results are presented as average Nusselt numbers against Péclet number. Minimum Nusselt numbers are found at some values of Péclet number in the mixed convection regime. The results show that, increasing H or/and K_r lead to increase of total average Nusselt number and render the solid and fluid towards thermal equilibrium conditions. The effects of Darcy number, Rayleigh number and porosity on average Nusselt numbers has been evaluated for different value of H and K_r or thermal conductivity ratio between solid and fluid (k_f/k_s). The results show that, the deterioration of heat transfer rate is more significant at higher values of Rayleigh number. The total average Nusselt number could be enhanced by increasing the value of porosity.

Keywords: Mixed convection; Jet impingement; Porous media; Numerical study; Thermal non-equilibrium

1. Introduction

Jet impingement of a cold fluid is an efficient cooling method of a heated surface and it has been used in many applications. The characteristics of jet impingement cooling through porous medium are becoming important. For example, turbine blade internal cooling, electronic cooling systems, solar collectors, etc. New applications of porous medium are being developed to enhance heat transfer. For instance, the use of porous heat sink in electronic cooling and the use of porous inserts in injection molding. The development towards miniaturization has required the electronic devices to be produced in small size and yet under high heat flux. However, high heat flux could induce buoyancy flow which brings adverse effects to heat transfer. Therefore, it is important to consider the buoyancy effects in designing an efficient impingement cooling system.

Generally, convection and heat transfer in porous media has been extensively investigated [1–4]. Jet impingement through pure fluid (non-porous) has been widely studied by many researchers [5–10] using direct air impingement onto a solid surface. However, jet impingement through porous media has received relatively less attention. Literatures [11,12] have shown that, jet impingement through porous medium could enhance the heat transfer rate as compared to that without porous medium.

Jeng and Tzeng [11] have investigated numerically the air impingement cooling of a porous metallic foam heat sink in the forced convection mode without considering the buoyancy effects. Their findings revealed that the heat transfer performance by using the porous Aluminum foam heat sink could be increased 2 to 3 times as compared to that without it. Jeng and Tzeng [13] have attempted to verify the numerical results by experiment. The results show that the heat transfer performance by using the porous Aluminum foam heat sink could be increased 3 to 5 times as compared to that without it.

* Corresponding author.
E-mail address: kok-cheong.wong@nottingham.edu.my (K.-C. Wong).

1290-0729/$ – see front matter
doi:10.1016/j.ijthermalsci.2008.06.004

Nomenclature

C_F	coefficient of friction
c_P	specific heat at constant pressure ..... $\mathrm{J\,kg^{-1}\,K^{-1}}$
D	half of the dimensionless width of the jet, $D = d/L$
d	half of the width of the jet (Fig. 1) ..... m
Da	Darcy number, $Da = K/L^2$
g	gravitational acceleration ..... $\mathrm{m\,s^{-2}}$
H	heat transfer coefficient parameter, $H = hL^2/k_f$
h	volumetric heat transfer coefficient between the solid and fluid in the porous medium $\mathrm{W\,m^{-3}\,K^{-1}}$
K	permeability of the porous medium ..... $\mathrm{m^2}$
K_r	porosity-scaled thermal conductivity ratio, $K_r = \varphi k_f/(1-\varphi).k_s$
k	thermal conductivity ..... $\mathrm{W\,m^{-1}\,K^{-1}}$
L	half of the heat source length (Fig. 1) ..... m
N	total number of nodes in the domain
Nu	local Nusselt number
$\overline{Nu}$	average Nusselt number along the heat source
P	dimensionless pressure, $P = p/\rho V_o^2$
p	pressure ..... Pa
Pe	Péclet number, $Pe = V_o L/\alpha_f$
Pr	Prandtl number, $Pr = \upsilon/\alpha_f$
q''	heat flux ..... $\mathrm{W\,m^{-2}}$
Ra	Rayleigh number for porous medium, $Ra = g\beta K(T_h - T_c)L/\upsilon\alpha_f$
S	dimensionless distance from the heated portion to the end of domain, $S = s/L$
s	distances from the end of heated portion to the end of domain (Fig. 1) ..... m
T	temperature ..... K
U, V	non-dimensional velocity components along X- and Y-axes, respectively, $U = u/V_0$, $V = v/V_0$
u, v	velocity components along x- and y-axes, respectively ..... $\mathrm{m\,s^{-1}}$
V_o	jet velocity ..... $\mathrm{m\,s^{-1}}$
X, Y	non-dimensional Cartesian coordinates, $X = x/L$, $Y = y/L$
x, y	Cartesian coordinates ..... m

Greek symbols

α	thermal diffusivity ..... $\mathrm{m^2\,s^{-1}}$
β	coefficient of thermal expansion ..... $\mathrm{K^{-1}}$
θ_f	non-dimensional fluid temperature, $\theta_f = \frac{T_f - T_c}{T_h - T_c}$
θ_s	non-dimensional solid temperature, $\theta_s = \frac{T_s - T_c}{T_h - T_c}$
μ	dynamic viscosity of fluid ..... $\mathrm{kg\,m^{-1}\,s^{-1}}$
υ	kinematic viscosity of fluid ..... $\mathrm{m^2\,s^{-1}}$
ρ	fluid density ..... $\mathrm{kg\,m^{-3}}$
Ψ	non-dimensional stream function
φ	porosity

Subscript

c	cold wall
h	hot wall
f	fluid phase
s	solid phase
t	total (fluid + solid)

Alkam et al. [14] numerically investigated the transient forced convection in the developing region of parallel-plate ducts with Brinkman–Forchheimer extended Darcy model. A high-thermal conductivity porous substrate is attached to the inner wall of one plate in order to enhance the heat transfer. Results show that for $Da < 10^{-4}$, the effect of microscopic inertial coefficient can be eliminated, while the effect of Da become not significant for microscopic inertial coefficient higher than 10^3. Heat transfer can be enhanced by using porous inserts with the properties of higher thermal conductivity, lower Da, and higher microscopic inertial coefficient.

Saeid and Mohamad [15] considered the buoyancy effects to study numerically the mixed convection regime in fluid saturated porous media with jet impingement cooling of a horizontal surface using Darcy model under thermal equilibrium condition. The results that are presented in the mixed convection regime shows that mixed convection may cause minimum heat transfer rate.

As a matter of fact, the local thermal equilibrium in convection in porous media is not valid for many cases as reported in the references [3,16] for different applications. Phanikumar and Mahajan [12] have examined the flow and heat transfer characteristics of high porosity metal foam samples heated from below. They have shown that, the results of non-thermal equilibrium model are in better agreement with experimental data as compared to thermal equilibrium model. Phanikumar and Mahajan [12] and Schumann [17], suggested a simple two equation model to account for non-equilibrium condition for incompressible forced flow in a porous medium.

The thermal non-equilibrium model has been applied in the investigation of different convection heat transfer problems [18–28] in porous media. In this thermal non-equilibrium modeling, it is required to know the thermo-physical properties of the solid and fluid phases, and the volumetric heat transfer coefficient between them. Recently, Saeid [22] has investigated numerically the interaction of the jet impingement with crossflow in a porous layer using the local thermal non-equilibrium model. The Darcy model is used in the formulation and the results are presented to show the effect of crossflow and the thermal non-equilibrium parameters.

The objective of the present study is to investigate the thermal characteristics of the jet impingement cooling with buoyancy effect in porous media in the mixed convection regime under local thermal non-equilibrium conditions. The Brinkman–Forchheimer–Darcy model is employed to enable the study of Darcian and non-Darcian effects. The physical model for this study is shown in Fig. 1. The upper surface is bounded by cold wall with temperature T_c; whereas the bottom surface is

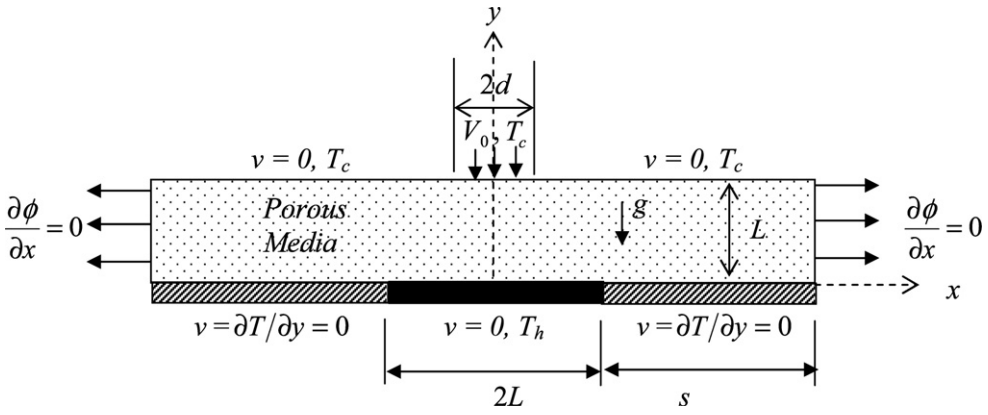

Fig. 1. Schematic diagram of the physical model and coordinate system.

bounded by heated surface with temperature T_h and adiabatic walls. The physical parameters in the present problem are the jet width $2d$, the jet velocity V_o, the temperature difference between the heat source and the jet, and the heat source length $2L$ which is assumed to be double of the distance from the jet. The jet width is assumed to be one tenth of the heat source length ($d/L = 0.1$). The Prandtl number for air ($Pr = 0.71$) is fixed throughout the numerical study. The coefficient of friction is fixed at $C_F = 0.1$ throughout the study.

2. Governing equations

The porous medium is assumed to be homogeneous and isotropic. The flow in the channel is assumed to be steady, laminar and incompressible. The thermophysical properties of the fluid and porous media are assumed to be constant. The Boussinesq approximation is used to approximate the density-temperature relation in the buoyancy term in the momentum equation. Under these assumptions, the conservation equations for mass, momentum and energy for the two-dimensional thermal non-equilibrium model are:

$$\frac{\partial u}{\partial x} + \frac{\partial v}{\partial y} = 0 \tag{1}$$

$$\frac{1}{\varphi^2}\left(\rho u\frac{\partial u}{\partial x} + \rho v\frac{\partial u}{\partial y}\right) = -\frac{dp}{dx} + \frac{\mu}{\varphi}\left(\frac{\partial^2 u}{\partial x^2} + \frac{\partial^2 u}{\partial y^2}\right) - \frac{\mu}{K}u - \frac{C_F\rho}{K^{1/2}}|v|u \tag{2}$$

$$\frac{1}{\varphi^2}\left(\rho u\frac{\partial v}{\partial x} + \rho v\frac{\partial v}{\partial y}\right) = -\frac{dp}{dy} + \frac{\mu}{\varphi}\left(\frac{\partial^2 v}{\partial x^2} + \frac{\partial^2 v}{\partial y^2}\right) - \frac{\mu}{K}v - \frac{C_F\rho}{K^{1/2}}|v|v + \rho\beta g(T_f - T_c) \tag{3}$$

$$(\rho c_P)_f\left(u\frac{\partial T_f}{\partial x} + v\frac{\partial T_f}{\partial y}\right) = \varphi k_f\left(\frac{\partial^2 T_f}{\partial x^2} + \frac{\partial^2 T_f}{\partial y^2}\right) + h(T_s - T_f) \tag{4}$$

$$(1-\varphi)k_s\left(\frac{\partial^2 T_s}{\partial x^2} + \frac{\partial^2 T_s}{\partial y^2}\right) + h(T_f - T_s) = 0 \tag{5}$$

where T_f denotes fluid phase temperature, and T_s denotes the solid phase temperature. Eqs. (1)–(5) are transformed into dimensionless governing equations (6)–(10) using the dimensionless parameters X, Y, U, V, θ_f and θ_s which are defined in the nomenclature.

$$\frac{\partial U}{\partial X} + \frac{\partial V}{\partial Y} = 0 \tag{6}$$

$$U\frac{\partial U}{\partial X} + V\frac{\partial U}{\partial Y} = -\varphi^2\frac{dP}{dX} + \frac{\varphi Pr}{Pe}\left(\frac{\partial^2 U}{\partial X^2} + \frac{\partial^2 U}{\partial Y^2}\right) - \frac{\varphi^2 Pr}{Da\,Pe}(U) - \frac{\varphi^2 C_F}{Da^{1/2}}U\sqrt{U^2+V^2} \tag{7}$$

$$U\frac{\partial V}{\partial X} + V\frac{\partial V}{\partial Y} = -\varphi^2\frac{dP}{dY} + \frac{\varphi Pr}{Pe}\left(\frac{\partial^2 V}{\partial X^2} + \frac{\partial^2 V}{\partial Y^2}\right) - \frac{\varphi^2 Pr}{Da\,Pe}(V) - \frac{\varphi^2 C_F}{Da^{1/2}}V\sqrt{U^2+V^2} + \frac{\varphi^2 Ra\,Pr}{Da\,Pe^2}\theta_f \tag{8}$$

$$U\frac{\partial \theta_f}{\partial X} + V\frac{\partial \theta_f}{\partial Y} = \frac{\varphi}{Pe}\left(\frac{\partial^2 \theta_f}{\partial X^2} + \frac{\partial^2 \theta_f}{\partial Y^2}\right) + \frac{H}{Pe}(\theta_s - \theta_f) \tag{9}$$

$$\left(\frac{\partial^2 \theta_s}{\partial X^2} + \frac{\partial^2 \theta_s}{\partial Y^2}\right) + \frac{HK_r}{\varphi}(\theta_f - \theta_s) = 0 \tag{10}$$

The governing parameters appeared in Eqs. (7)–(10) are defined as:

$$Ra = \frac{g\beta K(T_h - T_c)L}{\upsilon\alpha_f}, \qquad Pe = \frac{V_o L}{\alpha_f}, \qquad H = \frac{hL^2}{k_f}$$

$$K_r = \frac{\varphi k_f}{(1-\varphi)k_s}, \qquad Da = \frac{K}{L^2}, \qquad Pr = \frac{\upsilon}{\alpha_f} \tag{11}$$

The flow and heat transfer characteristics are symmetrical around Y-axis as shown in Fig. 1. Hence, one half is considered to be the computational domain. Based on this, the boundary conditions are:

At $X = 0$ (symmetry axis):

$$\frac{\partial \theta_s(0,Y)}{\partial X} = \frac{\partial \theta_f(0,Y)}{\partial X} = U(0,Y) = \frac{\partial V(0,Y)}{\partial X} = 0 \tag{12a}$$

At $X = 1 + S$ (flow exit):

$$\frac{\partial \theta_s(1+S,Y)}{\partial X} = \frac{\partial \theta_f(1+S,Y)}{\partial X} = \frac{\partial U(1+S,Y)}{\partial X} = \frac{\partial V(1+S,Y)}{\partial X} = 0 \tag{12b}$$

At $Y = 0$ (lower surface):

$$U(X,0) = 0, \qquad V(X,0) = 0$$
$$\theta_s(X,0) = \theta_f(X,0) = 1 \quad \text{for } 0 \leqslant X \leqslant 1 \quad \text{and}$$
$$\frac{\partial \theta_s(X,0)}{\partial Y} = \frac{\partial \theta_f(X,0)}{\partial Y} = 0 \quad \text{otherwise} \tag{12c}$$

At $Y = 1$ (upper surface):

$$\theta_s(X,1) = \theta_f(X,1) = U(X,1) = 0$$
$$V(X,1) = -1, \quad \text{for } 0 \leqslant X \leqslant D \quad \text{and}$$
$$V(X,1) = 0 \quad \text{otherwise} \tag{12d}$$

The physical quantities for evaluating the heat transfer characteristics are the local and average Nusselt numbers along the heated surface for the fluid phase and solid phase which are defined as follow:

$$Nu_f = \frac{q''_f L}{\Delta T \varphi k_f} = \left(-\frac{\partial \theta_f}{\partial Y}\right)_{Y=0}$$
$$\overline{Nu}_f = \int_0^1 Nu_f \, dX \tag{13}$$
$$Nu_s = \frac{q''_s L}{\Delta T (1-\varphi) k_s} = \left(-\frac{\partial \theta_s}{\partial Y}\right)_{Y=0}$$
$$\overline{Nu_s} = \int_0^1 Nu_s \, dX \tag{14}$$

where $\Delta T = T_h - T_c$, q''_f and q''_s are the heat flux for fluid and solid phase, respectively.

3. Numerical procedures

The momentum equations (7)–(8) and energy equations (9)–(10) are integrated numerically over control volumes using the finite volume method [29]. The power law scheme [29] is applied for the convection–diffusion formulation in Eqs. (7)–(9). The central differencing scheme is applied in diffusion equation (10). The SIMPLEC algorithm [30] for the pressure-velocity coupling is used in the present study. The resulting algebraic equations were solved sequentially by using line-by-line Tri-Diagonal Matrix Algorithm iteration. The iteration process is terminated if the following condition is satisfied:

$$\sum_{i,j} \left| \Phi^n_{i,j} - \Phi^{n-1}_{i,j} \right| \Big/ \sum_{i,j} \left| \Phi^n_{i,j} \right| \leqslant 5 \times 10^{-7} \tag{15}$$

where n denotes the iteration step, and Φ is the general dependent variable which can stands for θ_f, θ_s, U or V. Relaxation factors for U-velocity, V-velocity and pressure are employed to avoid divergence during the iteration. The grids are stretched in the X-direction, where steep variations in thermal and velocity fields are expected near the heat source. For the grids in Y-direction, finer mesh is fixed near the walls and coarser mesh near the core region.

Since there is no experimental result to validate the numerical results of present study, the energy balance method and grid independence test are used as a measure to verify the accuracy of the present numerical method and the results reported hereafter. The heat lost by the lower heated portion through solid and fluid phases must be equal to the sum of heat transferred to the upper cold portion through solid and fluid phases, and the heat being carried away by the fluid at the jet exit. Based on that, the following equation for energy balance is derived:

$$\frac{1}{K_r} \int_0^1 \left(-\frac{\partial \theta_s}{\partial Y}\right)_{Y=0} dX + \int_0^1 \left(-\frac{\partial \theta_f}{\partial Y}\right)_{Y=0} dX = \frac{1}{K_r} \int_0^{1+S} \left(-\frac{\partial \theta_s}{\partial Y}\right)_{Y=1} dX + \int_0^{1+S} \left(-\frac{\partial \theta_f}{\partial Y}\right)_{Y=1} dX + \int_0^1 Pe (U\theta_f)_{1+S} \, dY \tag{16}$$

Table 1
Comparison of the results at different mesh sizes with $Pe = Ra = 100$, $\varphi = 0.87$, $C_F = 0.1$ and $Da = 10^{-3}$

H	K_r	30×150		40×200		50×250	
		$\overline{Nu}_s$	$\overline{Nu}_f$	$\overline{Nu}_s$	$\overline{Nu}_f$	$\overline{Nu}_s$	$\overline{Nu}_f$
1	0.001	1.444	3.486	1.444	3.488	1.443	3.488
1	0.1	1.457	3.487	1.456	3.489	1.456	3.489
1	1	1.570	3.493	1.570	3.495	1.570	3.496
10	1	2.095	3.134	2.095	3.134	2.096	3.135
100	1	2.573	2.734	2.574	2.734	2.574	2.735
1000	1	2.652	2.658	2.653	2.659	2.653	2.660
1000	1000	3.570	3.570	3.575	3.575	3.576	3.576

Table 2
Comparison of the total average Nusselt number for different Pe values with $Ra = 100$, $\varphi = 0.87$, $C_F = 0.1$, $H = 1$, $K_r = 1$ and $Da = 10^{-3}$

Pe	30×150		40×200		50×250	
	$\overline{Nu}_s$	$\overline{Nu}_f$	$\overline{Nu}_s$	$\overline{Nu}_f$	$\overline{Nu}_s$	$\overline{Nu}_f$
1	1.484	3.322	1.483	3.325	1.483	3.327
10	1.497	3.508	1.497	3.509	1.496	3.510
40	1.525	2.948	1.525	2.949	1.525	2.951
100	1.570	3.493	1.570	3.495	1.570	3.495
500	1.681	6.627	1.680	6.647	1.680	6.655
1000	1.719	9.598	1.719	9.671	1.719	9.707

The results of grid independence test for different mesh sizes are presented in Table 1 for various values of H and K_r at fixed $Pe = Ra = 100$ and $Da = 10^{-3}$. The discrepancy in the values of $\overline{Nu}_s$ or $\overline{Nu}_f$ among the 3 mesh sizes is less than 0.2%. The grid independence is checked for different values of Pe. Table 2 presents $\overline{Nu}_s$ and $\overline{Nu}_f$ for 3 mesh sizes for different Pe at fixed $Ra = 100$, $Da = 10^{-3}$, $H = 1$ and $K_r = 1$. The highest discrepancy in average Nusselt numbers are found at $Pe = 1000$ for $\overline{Nu}_f$ when compared between (30×150) and (50×250) which is 1.13%, whereas the discrepancy between the mesh (40×200) and (50×250) is 0.75%. Therefore, the mesh size (40×200) is considered good enough to generate grid independence results. Furthermore, the maximum error of energy balance (the per-

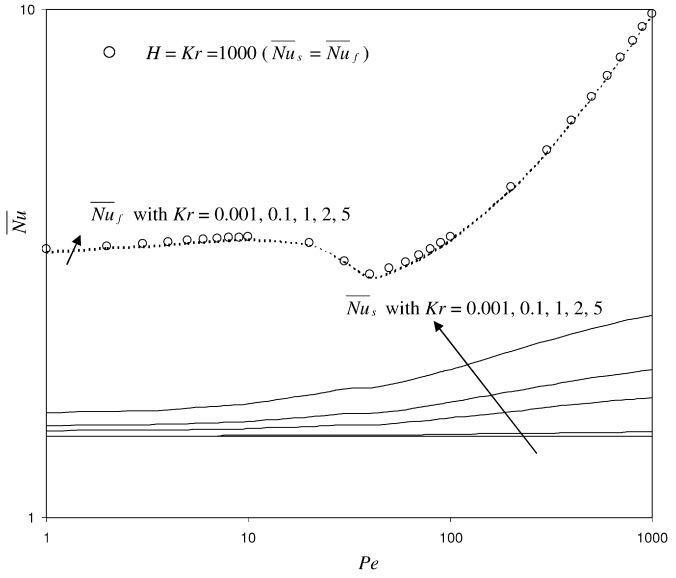

Fig. 2. Variation of average Nusselt numbers against Pe with $H = 1$, $Ra = 100$, $\varphi = 0.87$ and $Da = 10^{-3}$.

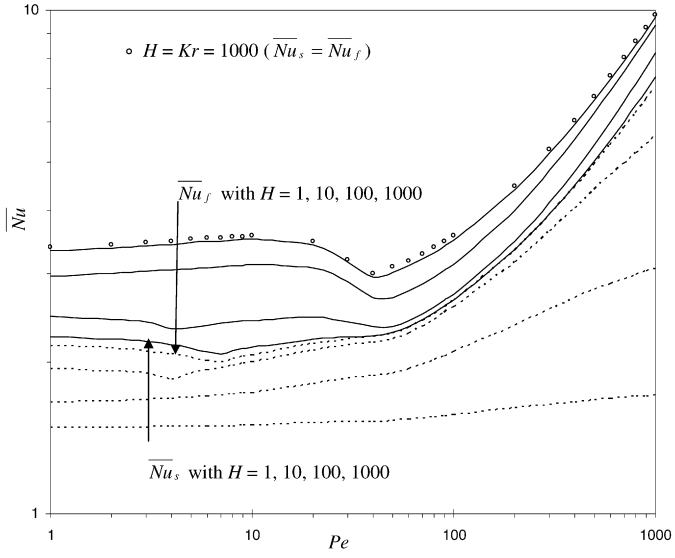

Fig. 3. Variation of average Nusselt numbers against Pe with $K_r = 1$, $\varphi = 0.87$, $Ra = 100$ and $Da = 10^{-3}$.

centage of difference between the left-hand side and right-hand side of Eq. (16)) is found to be less than 1%.

4. Results and discussion

The results are presented as average Nusselt numbers against Péclet number for different values of the governing parameters for the range of $1 \leqslant Pe \leqslant 10^4$, $10 \leqslant Ra \leqslant 200$, $10^{-6} \leqslant Da \leqslant 10^{-3}$, $0.75 \leqslant \varphi \leqslant 0.99$, $0.001 \leqslant K_r \leqslant 5$ and $1 \leqslant H \leqslant 10^3$. The ranges of governing parameters selected above are able to demonstrate the mixed convection regime for the Darcy and non-Darcy regime under thermal non-equilibrium as well as thermal equilibrium between the solid and fluid phases.

Previous studies [18–28] used the thermal non-equilibrium model for investigating different convective heat transfer problems. These studies found that the local thermal equilibrium condition can be satisfied with high values of porosity scaled thermal conductivity ratio parameter (K_r) and heat transfer coefficient parameter (H). The porous medium such as metal foam has low thermal conductivity of fluid compared to that of solid, which gives low values of K_r. Porous medium with low K_r will render more heat to be carried away by heat conduction through solid rather than heat convection through fluid. The porous medium considered for the present study is of high porosity ranging between $0.75 \leqslant \varphi \leqslant 0.99$. The porous metal foams [13,31,32] are normally fall within this range, and varying the porosity within this range will vary K_r within the range of $3k_f/k_s \leqslant K_r \leqslant 99k_f/k_s$. Higher values of porosity or higher k_f/k_s ratio will lead to higher value of K_r. Fig. 2 shows the variation of average Nusselt number for both fluid and solid against Péclet number for different K_r values with fixed values of $H = 1$, $Ra = 100$, $\varphi = 0.87$ and $Da = 10^{-3}$. In this case, it is assumed that, variation of K_r is solely attributed to the variation in k_f/k_s ratio since the porosity is fixed at $\varphi = 0.87$. In Fig. 2, the logarithmic scale is used for both $\overline{Nu}$ and Pe. It is noticed that, for any given value of Pe, $\overline{Nu}_f$ is almost unchanged with the increase in K_r. Increasing k_s leads to decrease in K_r. However, increasing k_s give negligible effect on $\overline{Nu}_f$ for low value of heat transfer coefficient parameter ($H = 1$) as the heat transfer between the solid and fluid is poor. The value of $\overline{Nu}_f$ is normally higher than $\overline{Nu}_s$ as heat transfer through convective cold fluid is normally more efficient than conduction through solid unless fluid and solid are under thermal equilibrium. At $H = 1$ (low value of H), the fluid phase temperature has minimum effect on the solid phase temperature. At low value of K_r, thermal resistance of solid is low compared to fluid, rendering major heat transfer through solid. Therefore, $\overline{Nu}_s$ is becoming approximately constant as K_r reduces to low value, and it increases with the increase in K_r. The increase in K_r leads to better thermal communication between the two phases. Therefore, the increase in K_r will result in the increase in $\overline{Nu}_s$ approaching towards the value of $\overline{Nu}_f$. It can be noticed in Fig. 2 and Table 1 that, as K_r increases, the difference between $\overline{Nu}_f$ and $\overline{Nu}_s$ is becoming smaller. The values of $\overline{Nu}_f$ and $\overline{Nu}_s$ become identical for high values of H and K_r ($H = K_r = 1000$) which shows thermal equilibrium condition. The results for $H = K_r = 1000$ are presented in Fig. 2 as a reference of thermal equilibrium condition although $K_r = 1000$ is not a practical value with air as convective fluid. Minimum $\overline{Nu}_f$ are found for all values of K_r at $Pe = 40$ as shown in Fig. 2. These minimum Nusselt numbers are due to the occurrence of opposing mixed convection that causes deterioration in heat transfer rate [15,33]. The present problem of jet impingement with buoyancy effects results in opposing mixed convection where the jet impinges vertically downward and the buoyancy force acts upward. When both buoyancy force (at certain high value of Rayleigh number) and strength of the jet are comparable (at certain Peclet number), the opposing mixed convection will be significant such that, the heat transfer rate for opposing mixed convection is lower than that of natural and forced convection.

The variation of average Nusselt number for both fluid and solid against Péclet number for different values of H is pre-

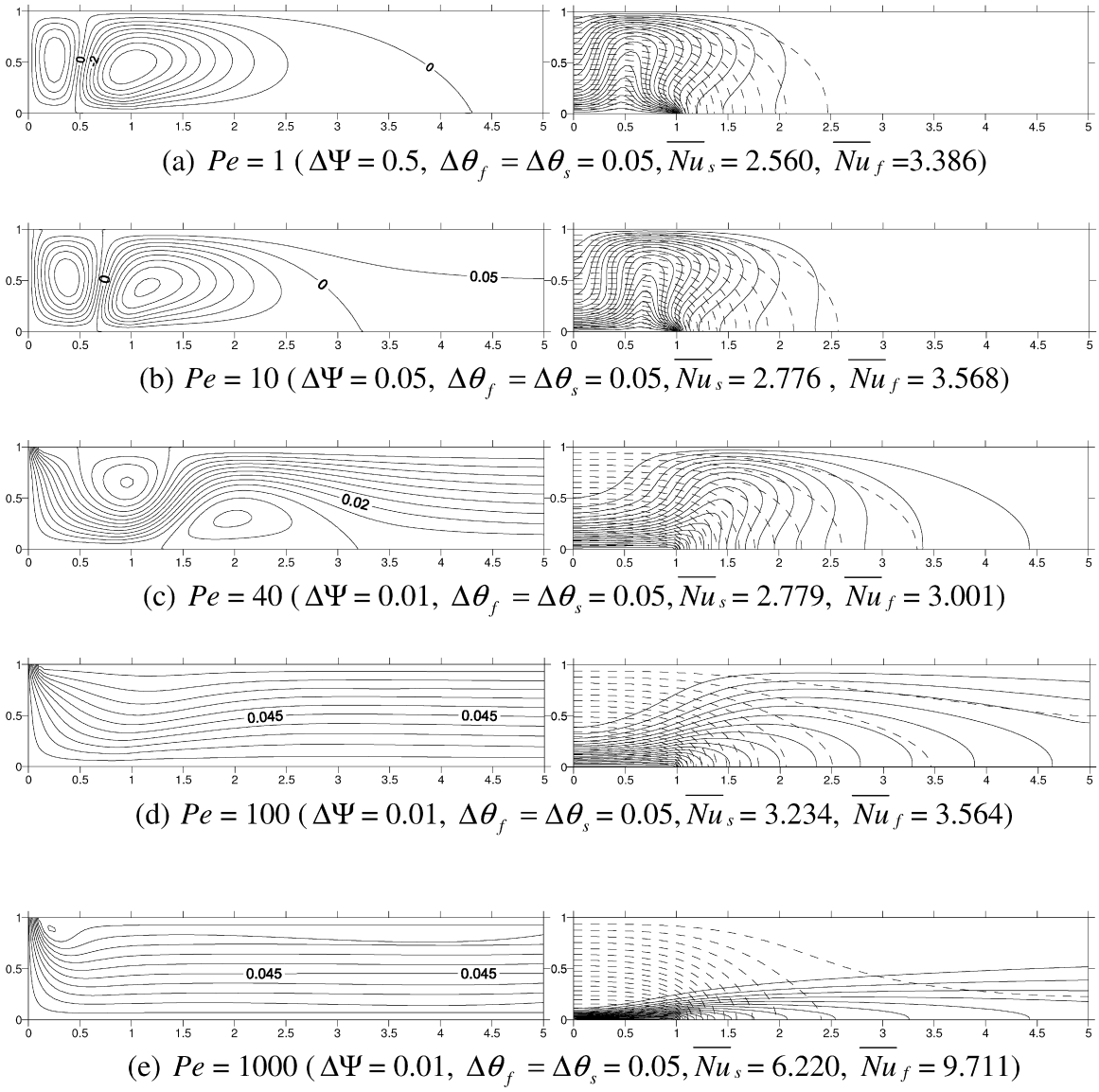

(a) $Pe = 1$ ($\Delta\Psi = 0.5$, $\Delta\theta_f = \Delta\theta_s = 0.05$, $\overline{Nu}_s = 2.560$, $\overline{Nu}_f = 3.386$)

(b) $Pe = 10$ ($\Delta\Psi = 0.05$, $\Delta\theta_f = \Delta\theta_s = 0.05$, $\overline{Nu}_s = 2.776$, $\overline{Nu}_f = 3.568$)

(c) $Pe = 40$ ($\Delta\Psi = 0.01$, $\Delta\theta_f = \Delta\theta_s = 0.05$, $\overline{Nu}_s = 2.779$, $\overline{Nu}_f = 3.001$)

(d) $Pe = 100$ ($\Delta\Psi = 0.01$, $\Delta\theta_f = \Delta\theta_s = 0.05$, $\overline{Nu}_s = 3.234$, $\overline{Nu}_f = 3.564$)

(e) $Pe = 1000$ ($\Delta\Psi = 0.01$, $\Delta\theta_f = \Delta\theta_s = 0.05$, $\overline{Nu}_s = 6.220$, $\overline{Nu}_f = 9.711$)

Fig. 4. Streamlines (left) and isotherms (right) for solid phase (dash lines) and fluid phase (solid lines) for different values of Pe, with $\varphi = 0.87$, $C_F = 0.1$, $Ra = 100$, $Da = 10^{-3}$, and $H = 1$ and $K_r = 1$.

sented in Fig. 3 with fixed $K_r = 1$, $Ra = 100$, $\varphi = 0.87$ and $Da = 10^{-3}$. As the value of H increases, the difference between $\overline{Nu}_f$ and $\overline{Nu}_s$ becomes smaller and approaching towards thermal equilibrium case. This is due to increasing the heat transfer coefficient parameter between the solid and fluid leads to better heat transfer between the fluid and solid phase from whichever hotter phase to the colder phase, bringing the temperature of the fluid closer to solid. At $H = 1$ and $K_r = 1$, the values of $\overline{Nu}_f$ is far apart from $\overline{Nu}_s$, and $\overline{Nu}_s$ is becoming almost constant regardless of the value of Pe. It can be seen in Fig. 3 and Table 1 that, when H increases, the values of $\overline{Nu}_f$ decrease, accompanying by increase in $\overline{Nu}_s$, both $\overline{Nu}_f$ and $\overline{Nu}_s$ get closer towards each other. This signifies that, both the solid and fluid are brought towards thermal equilibrium if H increases. Minimum $\overline{Nu}_f$ can be seen in Fig. 3 at $Pe = 40$ for $H \leqslant 100$. These minimum $\overline{Nu}_f$ are due to the adverse effect of mixed convection.

To demonstrate the effect of mixed convection under thermal non-equilibrium, the streamlines and isotherms for both fluid and solid for $H = 1$ and $K_r = 1$ are presented in Fig. 4. The streamlines of the flow for $Pe = 1$ and $Pe = 10$ shown in Fig. 4 (a) and (b) indicate the domination of natural convection. The jet flow seeps from the jet entrance through the porous medium vertically downwards, and makes a turn flow near the heated segment, then seeps through the middle of the two vortices, eventually flow towards the exit. The jet flow for $Pe = 10$ seeps through a wider distance along the heated segment as compared to the flow for $Pe = 1$ as shown in Fig. 4 (a) and (b). The isotherms in Fig. 4 (a) and (b) show that thermal plumes are formed in location between the two vortices. Temperature gradient on the area covered by plume is typically low, and signifies poor heat transfer at the plume area. The plume for $Pe = 10$ is being pushed towards the right as compared to the plume for $Pe = 1$, indicating the stronger flow of $Pe = 10$

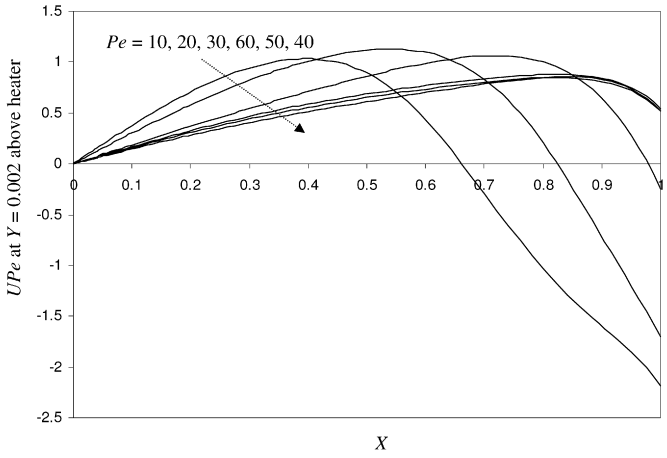

Fig. 5. Illustration of u-velocity with $U \times Pe$ at $Y = 0.002$ for different Pe at various distance X along the heater with $H = K_r = 1$, $Ra = 100$, $Da = 10^{-3}$, $\varphi = 0.87$.

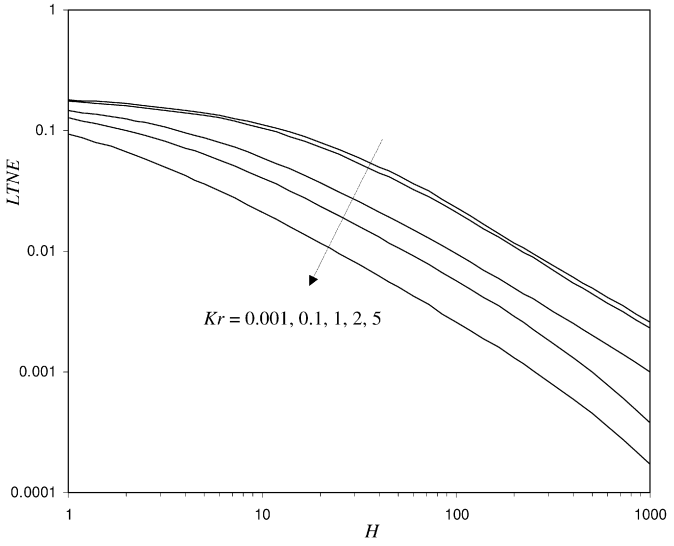

Fig. 6. Variation of *LTNE* against H for different K_r with fixed $\varphi = 0.87$, $Pe = Ra = 100$ and $Da = 10^{-3}$.

causing higher temperature gradient along the heated segment excluding the area occupied by the plume. Fig. 4(c) shows the flow of mixed convection for $Pe = 40$. Although the jet flow is stronger as compared to $Pe = 1$ and $Pe = 10$, the value of $\overline{Nu}_f$ drop significantly to 3.001 and obviously identified as minimum $\overline{Nu}_f$ along the curve shown in Fig. 3. The isotherms in Fig. 4(c) show that the plume disappears, but the overall temperature gradients along the heated segment drops. The dimensional u-velocities of the flow for $Pe = 10$–60 at the first grid point above the wall ($Y = 0.002$) are examined to find out the reason. It is a fact that, the magnitude or absolute value of $u(|u|)$ above the heated surface affects the heat transfer from the heated surface. Higher value of $|u|$ leads to higher heat transfer rate. u-velocity can be written as follow:

$$u = U V_0 = U(Pe\,\alpha_f/L) = U\,Pe(\alpha_f/L) \tag{17a}$$

$$uL/\alpha_f = U\,Pe \tag{17b}$$

Since the value of L/α_f is not specified in the present study and it is considered constant for a particular fluid and a particular physical model, comparison of u-velocity at different values of Pe can be made by comparing the dimensionless term uL/α_f which is equal to the value of $U \times Pe$ as shown in Eq. (17). The results of $U \times Pe$ are presented in Fig. 5. In the case of $Pe = 10$, the value of $U \times Pe$ is positive for $X < 0.66$ and negative for $X > 0.66$ due to the two vortices flowing in different direction. The mean value of $|U \times Pe|$ at the first grid point above the heater for the range of $0 \leqslant X \leqslant 1$ is defined as:

$$\overline{|U\,Pe|} = \int_0^1 |U\,Pe|\,dX \tag{18}$$

The mean values of $|U \times Pe|$ are calculated and the results are: 0.831, 0.745, 0.641, 0.543, 0.562, 0.589 for $Pe = 10, 20, 30, 40, 50, 60$, respectively. It is found that, the mean value of $|U \times Pe|$ is minimum for $Pe = 40$, which signifies the mean value of $|u|$ is minimum and heat transfer rate is minimum at this value of Pe. This is due to the effect of flow dispersion and buoyancy force at $Pe = 40$ that caused the minimum heat transfer rate. It can be seen that the streamlines for $Pe = 40$ shown in Fig. 4(c) is more widely spread near the jet entrance as compared to $Pe = 10$. The flow for $Pe = 40$ is being diverged into a wider but weaker flow as compared to the concentrated flow for $Pe = 10$. The buoyancy force which acted upward is strong enough to push the flow upward, causing minimum fluid flow through the heater surface, therefore minimizing the fluid velocity near the heater surface. As the value of Pe gets higher, the jet flow supersedes the strength of the buoyancy force, rendering increase in heat transfer rate. Fig. 4 (d) and (e) depicts the forced convection domination with streamlines and isotherms for $Pe = 100$ and $Pe = 1000$. The isotherms clearly show high fluid temperature gradient at $Pe = 100$ and $Pe = 1000$. In Fig. 4, the isotherms for solid are presented as dash line and the isotherms of fluid are presented as solid line. It is obvious that the isotherms between fluid and solid are much apart, signifying thermal non-equilibrium.

A better illustration of the effect of thermal local non-equilibrium parameters H and K_r are presented in Fig. 6 by introducing an evaluation parameter *LTNE* (local non-thermal equilibrium parameter) defined as:

$$LTNE = \frac{\sum_{N\text{-nodes}} |\theta_s - \theta_f|}{N} \tag{19}$$

where N is the total number of nodes in the domain. There are a total of 8000 nodes in the computation domain (200×40). *LTNE* is an indication of the average difference in dimensionless temperature between solid and fluid for one node in the domain. The solid and fluid are approaching thermal equilibrium if the value of *LTNE* is approaching zero. The results of *LTNE* are presented in Fig. 6 for different values of H and K_r with $Pe = Ra = 100$, $\varphi = 0.87$ and $Da = 10^{-3}$. The results show that, the increase in H or K_r will cause *LTNE* to decrease, and approaching towards thermal equilibrium between solid and fluid phases. Literally, the thermal equilibrium condition can be achieved by setting $H = K_r = 1000$ and the

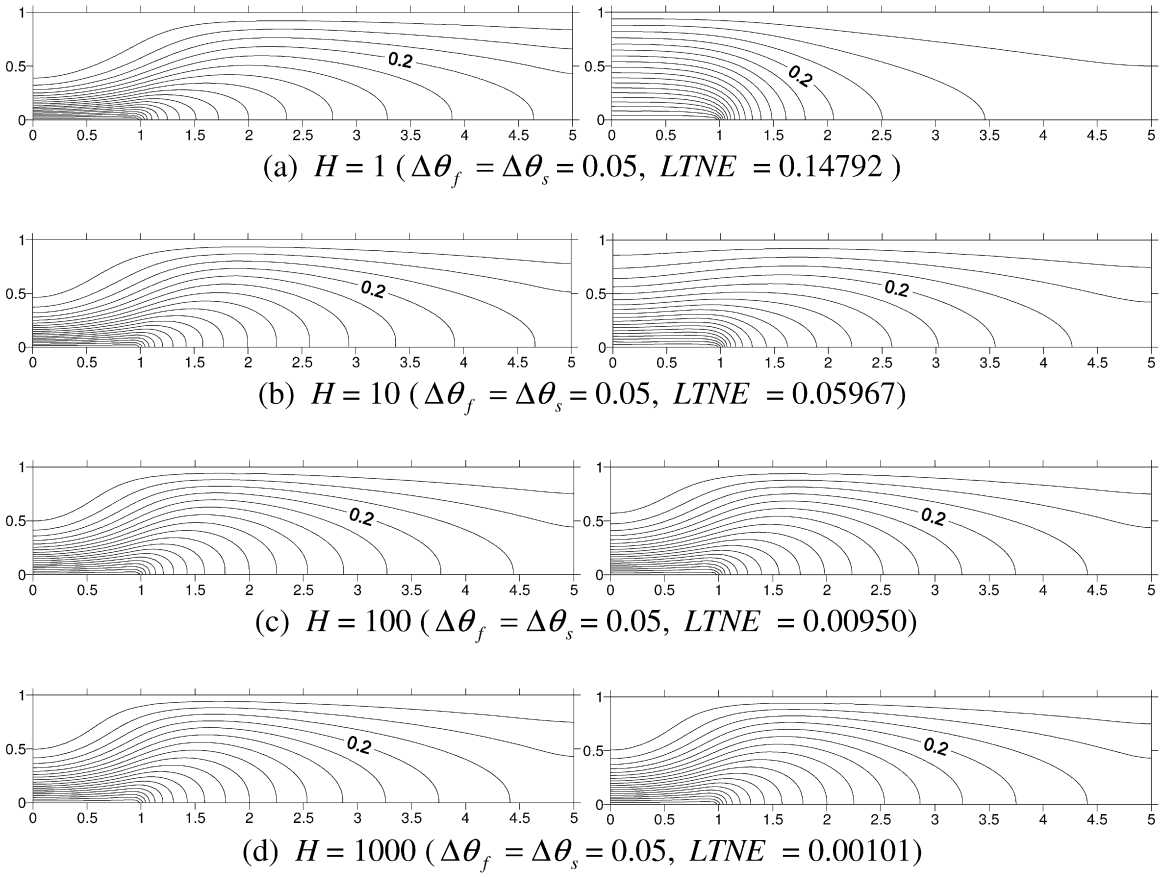

Fig. 7. Isotherms of fluid (left) and isotherms of solid (right) for different values of H with $K_r = 1$, $\varphi = 0.87$, $Pe = Ra = 100$, $Da = 10^{-3}$.

value of *LTNE* is found to be about 0.000001. It can be seen in Fig. 6, for any value of K_r presented, the value of *LTNE* is less than 0.01 for $H = 1000$. The increase in K_r further reduces the value of *LTNE*. Therefore, increasing H or K_r will lead towards thermal equilibrium between solid and fluid phases. This is illustrated with isotherms in Fig. 7 for different H with $K_r = 1$, $\varphi = 0.87$, $Pe = Ra = 100$ and $Da = 10^{-3}$. It should be noted that, the streamlines for $Pe = 100$ in Fig. 7(a) is identical to the streamlines presented in Fig. 4(d). Fig. 7(a) shows the isotherms for $K_r = H = 1$ which demonstrated very high *LTNE* (*LTNE* = 0.14792) or big difference in solid and fluid temperatures. The isotherms of fluid phase show high temperature gradient near heat source. However, the isotherms of solid phase demonstrate heat conduction domination with quite uniform isotherms near the heat source with low temperature gradient. It can be observed in Fig. 7 (b), (c) and (d) that as the value of H increases, the isotherms of solid phase in the vicinity of heat source become closer, leads to increase in temperature gradient and increase in $\overline{Nu}_s$. Besides, as H increases, the difference between solid and fluid temperatures become smaller, justifies by the decrease in the values of *LTNE* as presented in Fig. 7. Fig. 7 (c) and (d) shows the isotherms for $H = 100$ (*LTNE* = 0.00950) and $H = 1000$ (*LTNE* = 0.00101) respectively which the isotherms for solid and fluid are identical, and the value of *LTNE* are less than 0.01 which may be small enough to be considered as thermal equilibrium.

Saeid [22] has used the similar physical model for the study of jet impingement with crossflow. He has derived and evaluated the average total heat transfer from the heated portion by assuming the heat transfer in the fluid and solid phases are entirely in parallel based on heat source length of $2L$. Reference to that, the average total heat transfer is obtained for the present symmetrical model illustrated in Fig. 1 by considering half of the heat source length L:

$$\overline{q_t''} = \frac{1}{L}\int_0^L q_t''(x)\,dx = -\frac{1}{L}\int_0^L \left\{\varphi k_f \left(\frac{\partial T_f}{\partial y}\right)_{y=0} + (1-\varphi)k_s\left(\frac{\partial T_s}{\partial y}\right)_{y=0}\right\} dx \quad (20)$$

The total average Nusselt number can be defined as follow:

$$\overline{Nu_t} = \frac{\overline{q_t''}L}{(T_h - T_c)\{\varphi k_f + (1-\varphi)k_s\}} = \frac{-1}{(K_r+1)}\left\{\int_0^1 K_r\left(\frac{\partial\theta_f}{\partial Y}\right)_{Y=0} dX + \int_0^1 \left(\frac{\partial\theta_s}{\partial Y}\right)_{Y=0} dX\right\} \quad (21)$$

The evaluation of total average Nusselt number is important to understand the total heat transfer rate of both solid and fluid

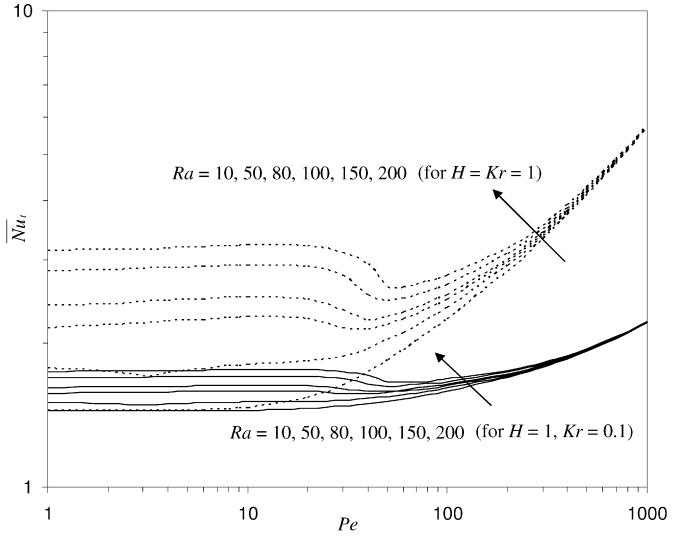

Fig. 8. Variation of total average Nusselt number against *Pe* for different *Ra* with $\varphi = 0.87$ and $Da = 10^{-3}$.

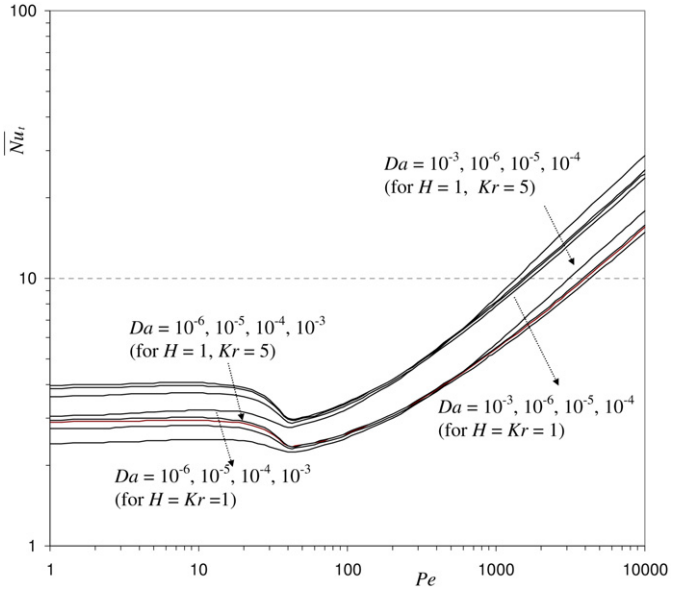

Fig. 9. Variation of total average Nusselt number against *Pe* for different *Da* with $\varphi = 0.87$ and $Ra = 100$.

phases, and it signifies the total performance of heat transfer for this jet impingement system through porous medium. The total average Nusselt number is evaluated for different values of *Ra*, *Da* and φ against the variation of *Pe*. The results are presented in Figs. 8 to 12.

The total average Nusselt number ($\overline{Nu_t}$) variation with *Pe* for different *Ra* and K_r are presented in Fig. 8 with $H = 1$, $\varphi = 0.87$ and $Da = 10^{-3}$. Minimum $\overline{Nu_t}$ is not obvious for $Ra = 10$ and $Ra = 50$ (Fig. 8). The higher the value of *Ra*, the more obvious the minimum $\overline{Nu_t}$ is. This is clearly shown in Fig. 8 at $Pe = 40$ to $Pe = 50$ for $Ra \geqslant 80$. At these values of *Pe*, the flow patterns are the same as that presented in Fig. 4(c), indicating thorough mixed convection. For $Pe \leqslant 300$, the buoyancy effect is significant. The increase in *Ra* increases $\overline{Nu_t}$ due to the increase in buoyancy force. The effect of *Ra* gradually

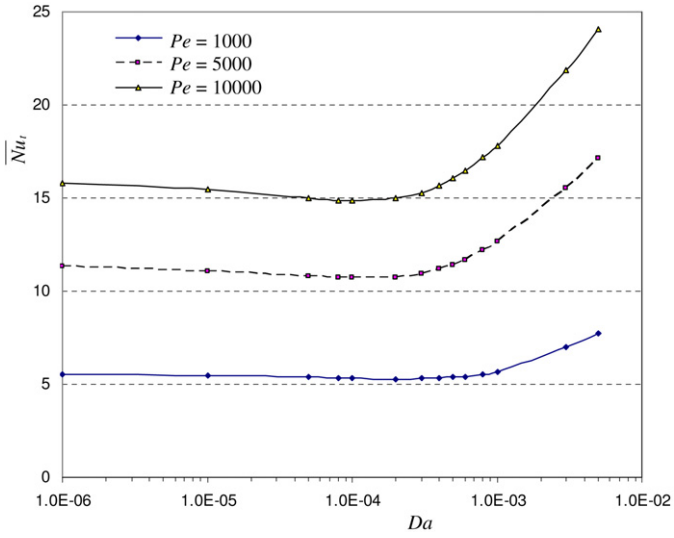

Fig. 10. Variation of total average Nusselt number against *Da* for different *Pe* with $H = K_r = 1$, $\varphi = 0.87$ and $Ra = 100$.

diminished for $Pe > 300$ as buoyancy effect is destroyed by the strong jet flow, and the curves for different *Ra* are forming a straight line as seen in Fig. 8. The transition from natural convection to mixed convection occurs when the value of *Pe* is increased gradually from low value to the significant region of $20 < Pe < 300$, and finally transition to forced convection occur when *Pe* exceeding 300. The present problem investigates the mixed convection regime in the range of $0.05 < Ra/Pe < 200$ which shows the transition of convection regimes clearly.

Fig. 9 depicts the effect of Darcy number on $\overline{Nu_t}$ variation with *Pe* and fixed $\varphi = 0.87$, $Ra = 100$ and $H = 1$. For both the values of K_r ($K_r = 1$ and $K_r = 5$), minimum $\overline{Nu_t}$ are found at $Pe = 40$ regardless of the value of *Da* and their flow patterns are similar to flow pattern in Fig. 4(c). As observed in Fig. 9, for $Pe < 40$, $\overline{Nu_t}$ decreases significantly with the increase in *Da*. This is similar to the results reported by Refs. [33,34] that the heat transfer rate decreases with increase in Darcy number in the low *Pe* or low Reynolds number region.

For $40 < Pe < 1000$, the variation of $\overline{Nu_t}$ with *Da* is not obvious especially for $Da = 10^{-6}$, 10^{-5} and 10^{-4} (Darcy regime) as shown in Fig. 9. The variation of $\overline{Nu_t}$ become obvious when $Pe > 1000$. The curve for $Da = 10^{-3}$ is observed to vary by crossing the curves of $Da = 10^{-6}$, 10^{-5} and 10^{-4} between the range of $400 \leqslant Pe \leqslant 700$, reversing the heat transfer characteristics when Darcy number increases to 10^{-3}. For $Pe > 800$, the values of $\overline{Nu_t}$ for $Da = 10^{-3}$ suddenly increase higher than that of $Da = 10^{-6}$, 10^{-5} and 10^{-4}. The variation is further investigated between the range of $Da = 10^{-6}$ to $Da = 5 \times 10^{-3}$ for $Pe = 1000, 5000, 10000$ and the results are presented in Fig. 10 for the case of $H = K_r = 1$. It is found for the all curves presented in Fig. 10, there exist a minimum $\overline{Nu_t}$ at certain value of *Da*. The minimum $\overline{Nu_t}$ (minimum points) are 5.299 (for $Pe = 1000$ at $Da = 2 \times 10^{-4}$), 10.071 (for $Pe = 5000$ at $Da = 10^{-4}$) and 14.853 (for $Pe = 10000$ at $Da = 10^{-4}$). For high *Pe* region, Fig. 10 indicates that $\overline{Nu_t}$ is approximately constant for the values of Darcy number before the minimum point (Darcy regime), and $\overline{Nu_t}$ increases significantly with the in-

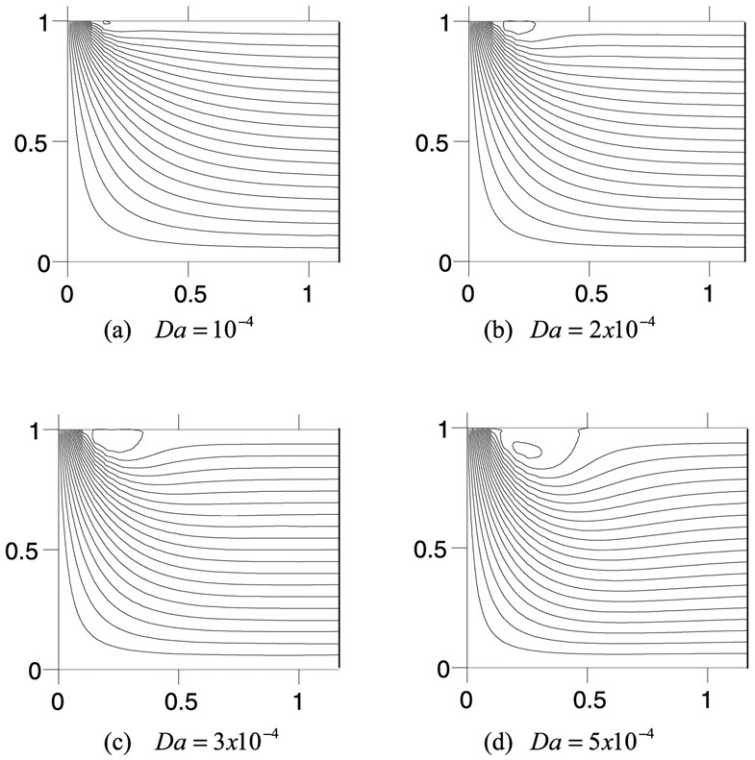

Fig. 11. Streamlines fluid phase for different values of Da with $Pe = 5000$, $H = K_r = 1$, $\varphi = 0.87$, and $Ra = 100$ ($\Delta\Psi = 0.005$).

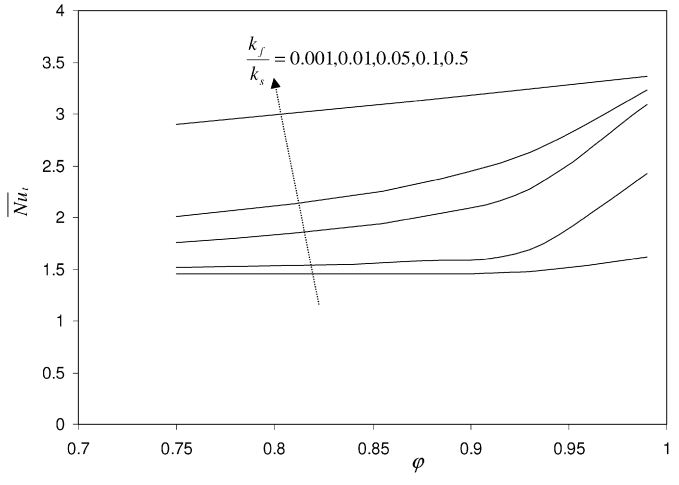

Fig. 12. Variation of total average Nusselt number against porosity with $Pe = Ra = 100$, $H = 1$ and $Da = 10^{-3}$.

crease in Darcy number after the minimum point (non-Darcy regime). The flow patterns of $Pe = 5000$ for different Darcy numbers in the vicinity of the region of minimum point are displayed in Fig. 11. The flow patterns in Fig. 11 (b)–(d) show that a vortex near the jet entrance is formed when the Darcy number is increased higher than $Da = 10^{-4}$. The onset of vortex formation occurs at $Da = 10^{-4}$ (the Darcy number that results in minimum $\overline{Nu_t}$) for $Pe = 5000$ as shown in Fig. 11(b). The vortex is formed as a result of entrainment by the jet flow with porous medium of higher porosity. It is observed in Fig. 11 that, the vortex formed at the jet entrance becomes bigger when the Darcy number increases. This is because the increase in Darcy number (the increase in permeability) reduces the pressure drop. The fluid that flow through porous medium experiences lower resistance. The medium with higher permeability allows fluid to penetrate with higher velocity and enhances the heat transfer rate in the forced convection regime. The flow patterns for $Pe = 1000$ and $Pe = 10000$ have been verified and they shows the same behavior with onset of vortex formation at $Da = 2 \times 10^{-4}$ and $Da = 10^{-4}$, respectively, and increase in size of vortex when Darcy number increases.

The effect of porosity on $\overline{Nu_t}$ is studied for various k_f/k_s ratio and fixed values of $Pe = Ra = 100$ and $Da = 10^{-3}$. It should be noted that, the porosity-scaled thermal conductivity ratio K_r is dependent on porosity. It is not appropriate to evaluate the effect of porosity with variation of K_r. Therefore thermal conductivity ratio k_f/k_s is presented instead of K_r. The results in Fig. 12 show that, for any given value of porosity, the increase in k_f/k_s enhances $\overline{Nu_t}$. The increase in porosity increases the value of $\overline{Nu_t}$. However, the effect of porosity become smaller when the value of k_f/k_s is small ($k_f/k_s = 0.001$) as the value of $\overline{Nu_t}$ becomes approximately constant. It is also found that the variation of H only causes small variation in the value of $\overline{Nu_t}$ for the range of k_f/k_s presented.

5. Conclusion

Jet impingement cooling through porous medium under thermal non-equilibrium has been investigated numerically. Mixed convection is demonstrated in the Darcy and non-Darcy regime. It can be concluded from this numerical study that, average Nusselt number for solid increases with the increase in poros-

ity scaled thermal conductivity ratio parameter whereas average Nusselt number for fluid remain approximately constant. The average Nusselt number for solid increases with the increase in heat transfer coefficient parameters while average Nusselt number for fluid decreases with the increase in heat transfer coefficient parameters. The results demonstrated the thermal equilibrium between solid and fluid at high values of porosity scaled thermal conductivity ratio parameter and heat transfer coefficient parameters. Therefore, the increase in porosity scaled thermal conductivity ratio parameter or heat transfer coefficient parameter brings the solid and fluids towards thermal equilibrium condition. The mixed convection behavior is found to be more significant for higher Rayleigh number. Minimum heat transfer rate are found occurring at some values of Péclet number due to the weak dispersed jet flow and interaction of buoyancy force which caused minimum fluid flow through the surface of the heater. The total average Nusselt number increases with the increase in k_f/k_s and porosity. The total average Nusselt number become approximately constant when the value of k_f/k_s is small.

References

[1] D.A. Nield, A. Bejan, Convection in Porous Media, third ed., Springer, New York, 2006.

[2] K. Vafai, Handbook of Porous Media, second ed., Marcel Dekker, New York, 2005.

[3] M. Kaviany, Principles of Heat Transfer in Porous Media, second ed., Springer, New York, 1999.

[4] I. Pop, D.B. Ingham, Convective Heat Transfer: Mathematical and Computational Modelling of Viscous Fluids and Porous Media, Pergamon, Oxford, 2001.

[5] H. Martin, Heat and mass transfer between impinging gas jets and solid surfaces, Advances in Heat Transfer 13 (1977) 1–60.

[6] K. Jambunathan, E. Lai, M.A. Moss, B.L. Button, A review of heat transfer data for single circular jet impingement, Int. J. Heat Fluid Flow 13 (1992) 106–115.

[7] I. Sezai, A.A. Mohamad, 3-D simulation of laminar rectangular impinging jets, flow structure and heat transfer, ASME J. Heat Transfer 121 (1999) 50–56.

[8] X. Li, J.L. Gaddis, T. Wang, Multiple flow patterns and heat transfer in confined jet impingement, Int. J. Heat Fluid Flow 26 (2005) 746–754.

[9] E. Arquis, M.A. Rady, S.A. Nada, A numerical investigation and parametric study of cooling an array of multiple protruding heat sources by a laminar slot air jet, Int. J. Heat Fluid Flow 28 (2007) 787–805.

[10] D. Sahoo, M.A.R. Sharif, Numerical modeling of slot-jet impingement cooling of a constant heat flux surface confined by a parallel wall, Int. J. of Thermal Science 43 (2004) 877–887.

[11] T.M. Jeng, S.C. Tzeng, Numerical study of confined slot jet impinging on porous metallic foam heat sink, Int. J. Heat Mass Transfer 48 (2005) 4685–4694.

[12] M.S. Phanikumar, R.L. Mahajan, Non-Darcy natural convection in high porosity metal foams, Int. J. Heat Mass Transfer 45 (2002) 3781–3793.

[13] T.M. Jeng, S.C. Tzeng, Experimental study of forced convection in metallic porous block subject to a confined slot jet, Int. J. Thermal Science 46 (2007) 1242–1250.

[14] M.K. Alkam, M.A. Al-Nimr, M.O. Hamdan, Enhancing heat transfer in parallel-plate porous inserts, Int. J. Heat Mass Transfer 44 (2001) 931–938.

[15] N.H. Saeid, A.A. Mohamad, Jet impingement cooling of a horizontal surface in a confined porous media: mixed convection regime, Int. J. Heat Mass Transfer 49 (2006) 3906–3913.

[16] K. Vafai, M. Sozen, Analysis of energy and momentum transport for fluid flow through a porous bed, ASME J. Heat Transfer 112 (1990) 690–699.

[17] T.E.W. Schumann, Heat transfer: a liquid flowing through a porous prism, J. Franklin Inst. 208 (1929) 405–416.

[18] K. Ichimiya, T. Matsuda, Y. Kawai, Effects of a porous medium on local heat transfer and fluid flow in a forced convection field, Int. J. Heat Mass Transfer 40 (7) (1997) 1567–1576.

[19] A. Amiri, K. Vafai, Analysis of dispersion effects and non-thermal equilibrium, non-Darcian, variable porosity incompressible flow through porous media, Int. J. Heat Mass Transfer 37 (1994) 939–954.

[20] A. Amiri, K. Vafai, Transient analysis of incompressible flow through a packed bed, Int. J. Heat Mass Transfer 41 (1998) 4259–4279.

[21] W.J. Minkowycz, A. Haji-Sheikh, K. Vafai, On departure from local thermal equilibrium in porous media due to a rapidly changing heat source: the Sparrow number, Int. J. Heat Mass Transfer 42 (1999) 3373–3385.

[22] N.H. Saeid, Jet impingement interaction with cross flow in horizontal porous layer under thermal non-equilibrium conditions, Int. J. Heat Mass Transfer 50 (2007) 4265–4274.

[23] S.J. Kim, S.P. Jang, Effect of the Darcy number, the Prandtl number, and the Reynolds number on local thermal non-equilibrium, Int. J. Heat Mass Transfer 45 (2002) 3885–3896.

[24] N. Banu, D.A.S. Rees, Onset of Darcy–Benard convection using a thermal non-equilibrium model, Int. J. Heat Mass Transfer 45 (2002) 2221–2228.

[25] A.C. Baytas, I. Pop, Free convection in a square porous cavity using a thermal non-equilibrium model, Int. J. Therm. Sci. 41 (2002) 861–870.

[26] A.A. Mohamad, Natural convection from a vertical plate in a saturated porous medium, non-equilibrium theory, J. Porous Media 4 (2001) 181–186.

[27] N.H. Saeid, Analysis of mixed convection in a vertical porous layer using non equilibrium model, Int. J. Heat Mass Transfer 47 (2004) 5619–5627.

[28] N.H. Saeid, A.A. Mohamad, Periodic free convection from a vertical plate in a saturated porous medium, non-equilibrium model, Int. J. Heat Mass Transfer 48 (2005) 3855–3863.

[29] S.V. Patankar, Numerical Heat Transfer and Fluid Flow, McGraw-Hill, New York, 1980.

[30] K. Versteeg, W. Malalasekera, An Introduction To Computational Fluid Dynamics: The Finite Volume Method, H. Pearson Higher Education, 1995.

[31] J.F. Liu, W.T. Wu, W.C. Chiu, W.H. Hsieh, Measurement and correlation of friction characteristic of flow through foam matrixes, Experimental Thermal Fluid Science 30 (4) (2006) 329–336.

[32] N. Dukhan, Correlations for the pressure drop for flow through metal foam, Experimental Fluids 41 (4) (2006) 665–672.

[33] K.C. Wong, N.H. Saeid, Numerical study of mixed convection on jet impingement cooling in a horizontal porous layer-using Brinkman-extended Darcy model, Int. J. Therm. Sci. 48 (1) (2009) 96–104.

[34] H.A. Hadim, G. Chen, Numerical study of non-Darcy mixed convection in a vertical porous channel, J. of Thermophysics 8 (1993) 371–373.